Supplement

To the manuscript: Biogeochemical versus biogeophysical temperature effects of historical land-use change in CMIP6

Amali A. Amali[1], Clemens Schwingshackl[1], Akihiko Ito[2], Alina Barbu[3], Christine Delire[3], Daniele Peano[4], David M. Lawrence[5], David Wårlind[6], Eddy Robertson[7], Edouard L. Davin[8,9,10], Elena Shevliakova[11], Ian N. Harman[12], Nicolas Vuichard[13], Paul A. Miller[6], Peter J. Lawrence[5], Tilo Ziehn[14], Tomohiro Hajima[15], Victor Brovkin[16,17], Yanwu Zhang[18], Vivek K. Arora[19], and Julia Pongratz[1,16]

Correspondence: Amali A. Amali (A.Amali@lmu.de)

This file includes:
S1: Model description and specifications,
S2: Supplementary tables S1 - S2
S3: Supplementary figures S1-S16

S1: Model Description and specifications

Across the constituent pools composing cLand, ESMs consistently depict a decline in the total carbon sequestered within carbon pools (Fig. 1a) with variability, in magnitude, across ESMs. The product pool (cProduct) is the only pool simulating an overall gain in carbon (sink) due to LUC (Fig. S1d). This aligns with expectations as cProduct constitutes product carbon (both short- and long-lived), often as an outcome of harvestings such as is used in housing and transport thus, includes carbon not yet in the atmosphere. For the change in vegetation carbon (ΔcVeg; Fig. S1a) the trends align more closely in the evolution, variance, and magnitude with the broader ΔcLand trends (Fig. 1a) in comparison to other carbon pools. A similar decrease is also modelled across the dynamic global vegetation models (DGVMs), with a spread that captures the upper bounds of the LUMIP estimates. Several ESMs simulate only minimal differences in carbon content between the simulations with and without land-use change. Spatially, a unanimous decrease in vegetation carbon pools (Fig. S3) is evident across the eastern U.S., the greater Indonesian region and some regions of West Africa, with differences across ESMs in the extent of this decline. Compared to their model counterparts, the EC-Earth3 models indicate marked vegetative carbon depletion across regions over Brazil and Argentina. Models including CNRM, the EC-Earth3 variants, GFDL, and UKESM also register notable vegetative carbon reductions over the North American Great Plains. Broadly, the models' historical land carbon emissions are dominated by the change in vegetation carbon, with the initial reduction due to deforestation offset in later decades by the increase due to enhanced uptake by CO_2 fertilisation and agricultural use of nitrogenous fertiliser. Therefore, while it is possible to attribute trends in ΔcLand across ESMs to be largely dominated by the contribution from ΔcVeg, this does not hold true for all the models. The presence of a crop harvest flux can also significantly impact vegetation carbon and/or soil carbon emissions, depending on how harvest is configured in each model. During harvest in CESM2, even though crop grain carbon is removed, the increased productivity of crops due to fertilisation, irrigation, and higher productivity plants actually leads to increases in soil carbon where crops are grown. This response is the opposite of what is observed in the real world, which is possibly due to lack of a representation of tillage in the model; tillage would likely lead to increased respiration, resulting in soil carbon losses. Further, what happens with soil carbon will depend on how much plant matter is removed during harvest; CLM5 assumes only grain is removed, but in reality, usually, more than just grain is removed during the harvest process (Lombardozzi et al., 2020). The MIROC model simulates the biogeochemical perturbation due to land-use change based on five types of land tiles in each land grid. Crop harvesting, nitrogen fixation by N-fixing crops, grazing pressure on pasture and rangeland, and the decay of organic matter in product pools are considered, all of which perturb the land biogeochemistry even when land use is fixed at pre-industrial conditions.

In estimating changes in soil carbon pools due to LUC, the consistency among ESMs in ΔcSoil remains subtle (Figs. S1b and S5). Shi et al. (2024) also recently revealed great divergence in ΔcSoil estimates simulated by CMIP6 models. In comparison to other models, only BCC and CNRM show a stark increase in ΔcSoil estimates due to LUC. However, the spread across the DGVM estimates indicates a decrease in soil carbon and captures most of the LUMIP models. Additionally, while other ESMs simulate a limited change at the beginning of the simulation (year 1850), GFDL is the only model to diverge from this trend in both vegetation (decrease) and soil (increase) carbon pools (Fig. S1a and b). An observed inflection across ESMs around 1900 can be seen to occur around 1970 for GFDL (Fig. S1b); a time when the ESMs already strongly diverge. A subset of models, however, show a declining trend in soil carbon pools over the eastern U.S., albeit characterised by varied magnitudes (Fig. S5). Distinctly, BCC, CNRM, and CESM2 exhibit increases in soil carbon pools due to LUC within the mid-latitudinal regions, while only the GFDL model estimates an increase in ΔcSoil over the Tibetan Plateau. Spatially, the increasing pattern in CNRM bears resemblance to that in CanESM5, but with opposing directions—depicting a decline rather than an increase. The LUC effect over the U.S. Great Plains is vivid in both BCC and CESM2's ΔcSoil simulations (Fig. S5). Notably, these changes in ΔcSoil contrast starkly with their respective vegetation (Fig. S3) and litter (Fig. S4) carbon pools, especially when compared to other models analysed. The EC-Earth3 models demonstrate a pairwise behaviour in their simulation of terrestrial carbon, with differences being traceable to their simulation of cLitter. We attribute this difference to an error of omission of coarse woody debris (cCwd) resulting in only leaf and fine root litter in the cLitter and cLand variables of EC-Earth3-Veg simulation used in this study (D. Wårlind, personal communication, July 24, 2023). CanESM5, sees a downward trend in soil carbon throughout the historical period that steepens in the final few decades. This is because in CanESM5 the soil decomposition rate over croplands is higher and the fraction of humified litter that is transferred to the soil carbon, as opposed to respired to the atmosphere, is lower than over natural vegetation. Consequently, as natural vegetation is replaced by croplands over the historical period, a decrease in global soil carbon is obtained, as is also seen in empirical measurements (Wei et al., 2014).

Spatial distributions of ESMs' representation of ΔcLitter (Fig. S4) reveal generally modest variations in litter carbon pools attributable to LUC. While other ESMs (EC-Earth3-CC, MIROC and MPI) show a decreasing pattern, a subset of ESMs (BCC, CNRM, and CanESM5), however, does indicate increases in cLitter in many regions of the world, particularly over the mid-western U.S. and Eastern Europe. A disparity is evident over the U.S. Great Plains, where EC-Earth3-CC shows a marked reduction of cLitter as opposed to a strong increase in CNRM. Contrarily, Boysen et al. (2020) reported analogous behaviour in cLitter estimates between EC-Earth3-Veg and CNRM in a global-scale deforestation experiment. Mirroring EC-Earth3- CC's simulation, both MIROC and MPI show a global decline across litter carbon pools, with these models being unique in signifying an upsurge in cLitter stocks across western Europe. It is pertinent to note that, owing to model architecture, neither the GFDL nor UKESM accounts for carbon transitions to litter carbon pools.

S2: Supplementary tables

Table S1: Dynamic global vegetation models used to compare LUMIP land-use change derived estimates in carbon stored in vegetation(cVeg) and soil (cSoil).

Model	References
CABLE-POP	Haverd et al. (2018)
CLASSIC	Melton et al. (2020); Asaadi et al. (2018)
CLM5.0	Lawrence et al. (2019)
DLEM	Tian et al. (2011, 2015)
IBIS	Yuan et al. (2014)
ISAM	Jain et al. (2013); Meiyappan et al. (2015); Shu et al. (2020)
ISBA-CTRIP	Delire et al. (2020)
JSBACH	Mauritsen et al. (2019); Reick et al. (2021)
JULES-ES	Wiltshire et al. (2021); Sellar et al. (2019); Burton et al. (2019)
LPJ-GUESS	Smith et al. (2014)
LPJmL	Schaphoff et al. (2018); von Bloh et al. (2018); Lutz et al. (2019) (tillage); Heinke et al. (2023) (livestock grazing)
LPJ-wsl	Poulter et al. (2011)
LPX-Bern	Lienert and Joos (2018)
ORCHIDEEv3	Krinner et al. (2005); Zaehle and Friend (2010); Vuichard et al. (2019)
SDGVM	Woodward and Lomas (2004); Walker et al. (2017)
VISIT	Ito and Inatomi (2012); Kato et al. (2013)
YIBs	Yue and Unger (2015)

Table S2: Biogeophysical and Biogeochemical effects of historical land use change estimated by previous studies. Data used to create Fig. 7. EMIC represents Earth system model of intermediate complexity while GCM represents Global Climate Model.

Reference	Time Frame	Models(s)	BGP effect (°C)	BGP effect (°C)	Carbon Stock (PgC)
Brovkin et al. (2004)	1800 - 2000	EMIC (CLIMBER-2-LPJ)	-0.26	0.18	-
Matthews et al. (2004)	1700 - 2000	EMIC (UVic ESCM)	-0.16	0.3	-
Brovkin et al. (2006)	1700 - 1992	EMIC (6 models)	-0.13 to -0.25	-	-
Davin et al. (2007)	1860 - 1992	IPSL-CM4	-0.05	-	-
Shi et al. (2007)	1700 - 1992	EMIC (MPM-2)	-0.09 to -0.16	-	-
Pongratz et al. (2009)	1850 - 2000	EMIC (ECHAM5)	-	-	-171
Pongratz et al. (2010)	800 – 2000	EMIC (ECHAM5)	-0.03	0.18	-
Lawrence et al. (2012)	1850 – 2005	CMIP5 (CCSM4)	-0.1	0.23	- 128
Eby et al. (2013)	1000 – 2000	EMIC (15 models)	-0.2	-	-
Wang et al. (2014)	1000 – 2000	EMIC (MPI-2)	-0.08	-	
Simmons and Matthews (2016)	1750 – 2000	EMIC (UVic ESCM v.2.9)	-0.24	0.22	-110
IPCC estimates Jia et al. (2019)	Multiple periods	Mean of GCMs	-0.1	0.2	
Devaraju et al. (2022)	1850 – 2005	ESM (CESM1)	-0.15	0.24	-133
Friedlingstein et al. (2023)	1850 – 2014	DGVMs (20 models)	-	-	-210
This study	**1850 – 2014**	**ESMs (13 models)**	**-0.03**	**0.20**	**-122**

S3: Supplementary figures

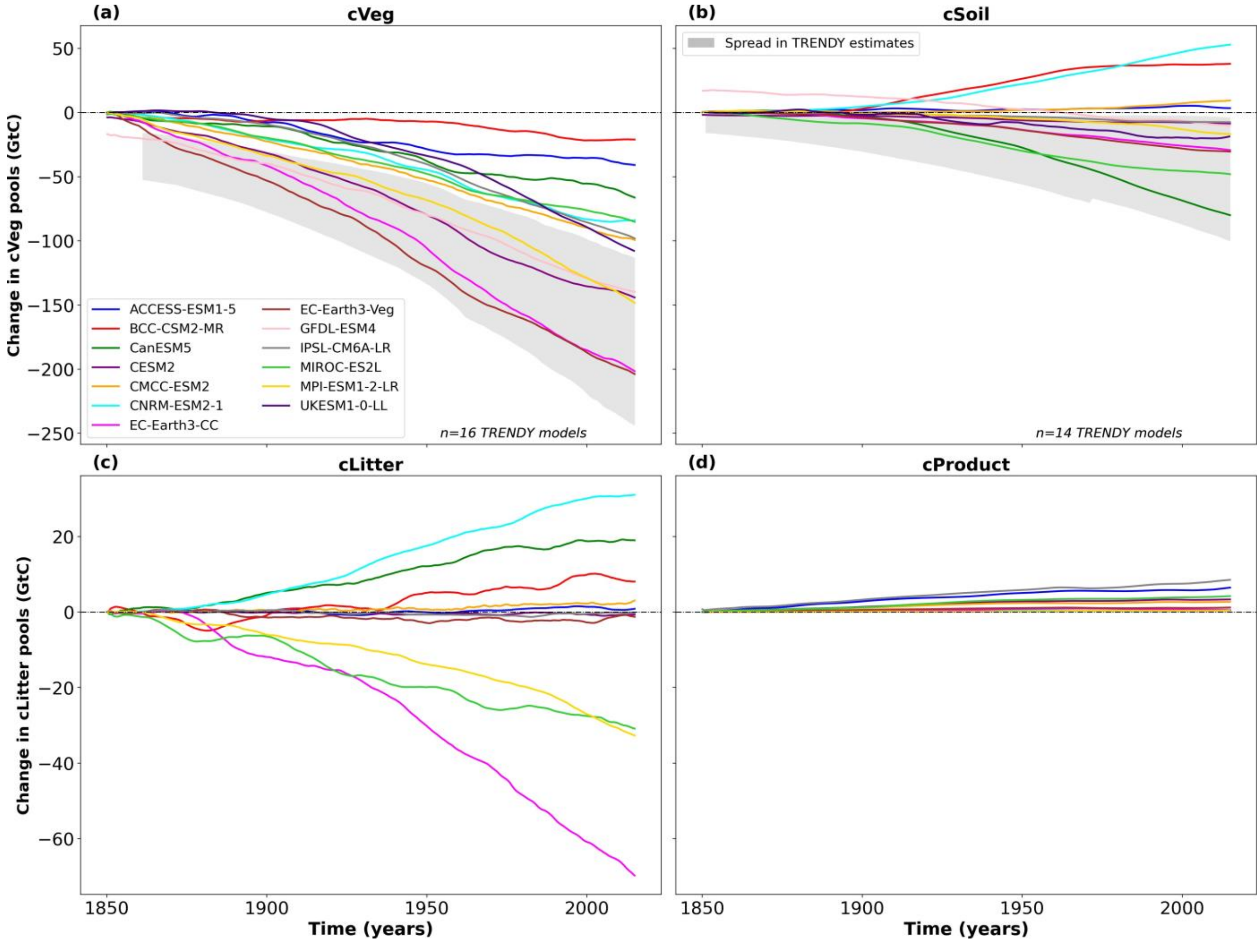

Figure S1. Response of carbon pools to land-use change (LUC) in (**a**) vegetation carbon pools (cVeg), (**b**) soil carbon pools (cSoil), (**c**) litter carbon pools (cLitter), and **d**) product carbon pools (cProduct) due to LUC for different Earth System Models in 1850-2014. A 10-year running average is applied across all plots. Grey shading in panels (**a**) and (**b**) represents the spread in the dynamic global vegetation models (DGVMs), computed as the standard deviation, across 16 and 14 model estimates, respectively of the "Trends and drivers of the regional-scale sources and sinks of carbon dioxide" (TRENDY v11; Sitch et al., 2015) dataset. LUC in TRENDY is computed as the difference between the S2 (without LUC) and S3 (with LUC) simulations. Note that the y-axis of panels (**c**) and (**d**) differ from the y-axis of panels (**a**) and (**b**).

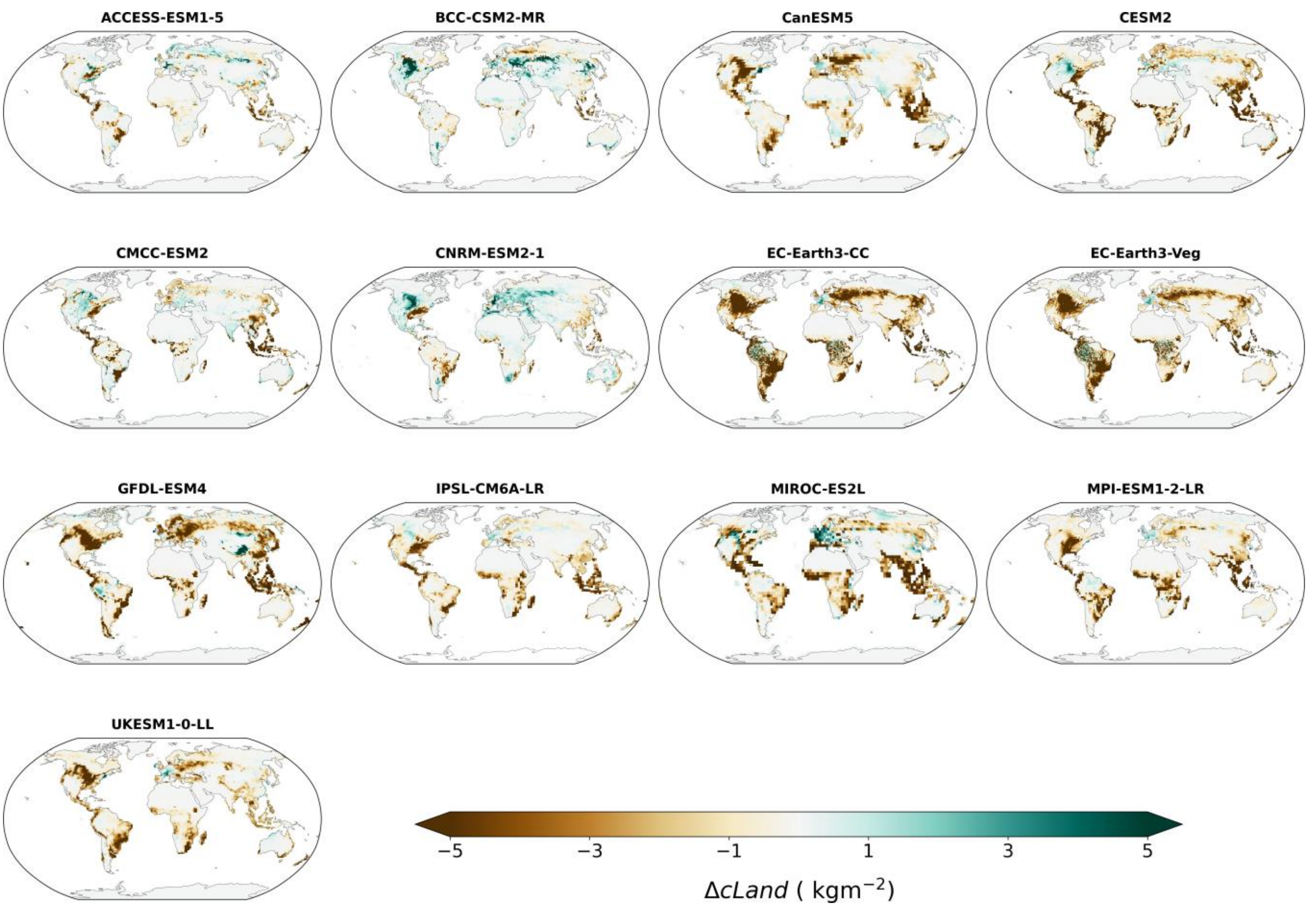

Figure S2. Change in total land carbon pools (ΔcLand) due to land-use change. Results are computed as the mean centred over the last 30 years (1985–2014), from the difference between *historical* and *hist-noLu* simulations.

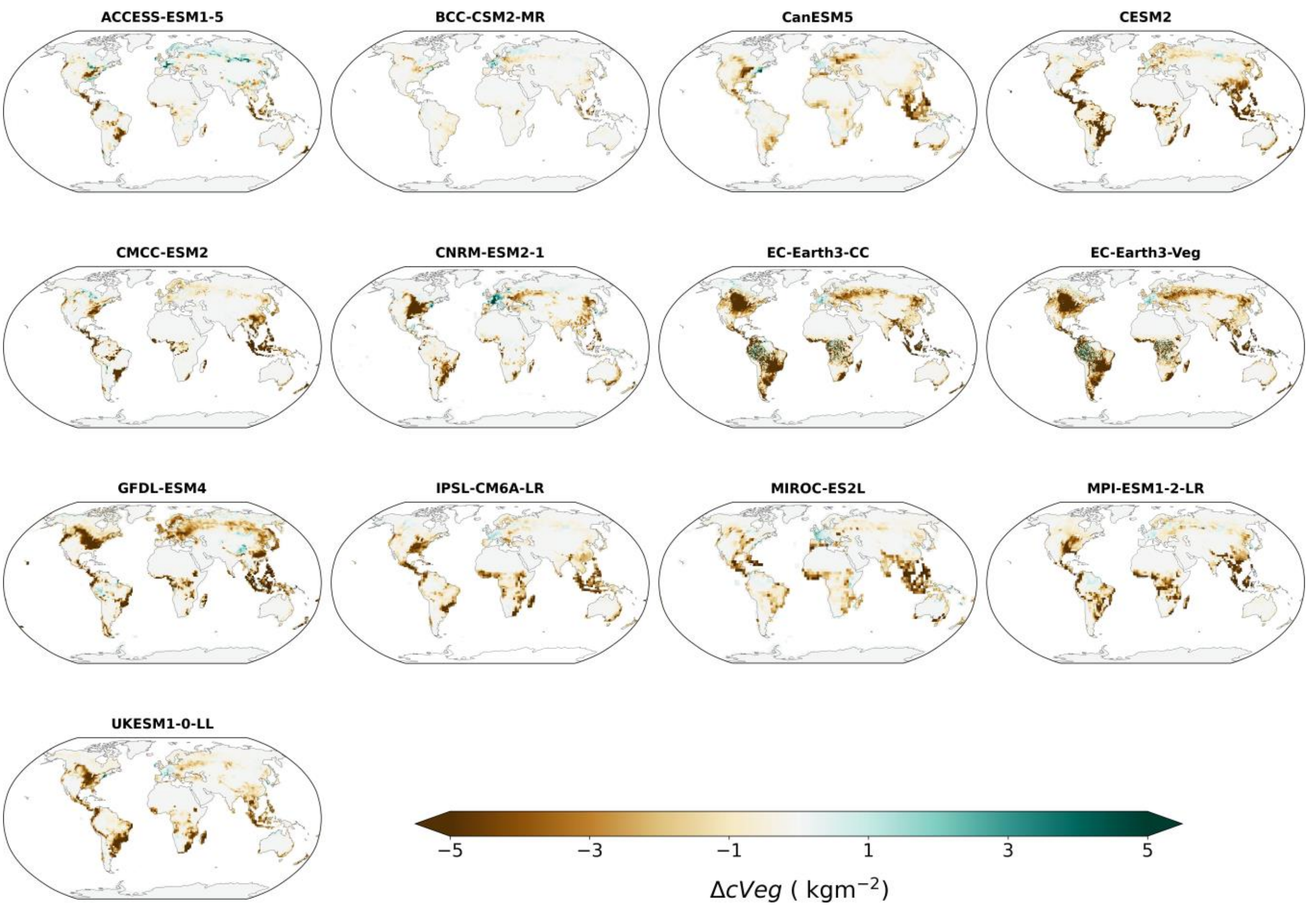

Figure S3. Change in vegetation carbon pools (ΔcVeg) due to land-use change. Results computed as the running mean, centred over the last 30 years (1985–2014), from the difference between *historical* and *hist-noLu* simulations.

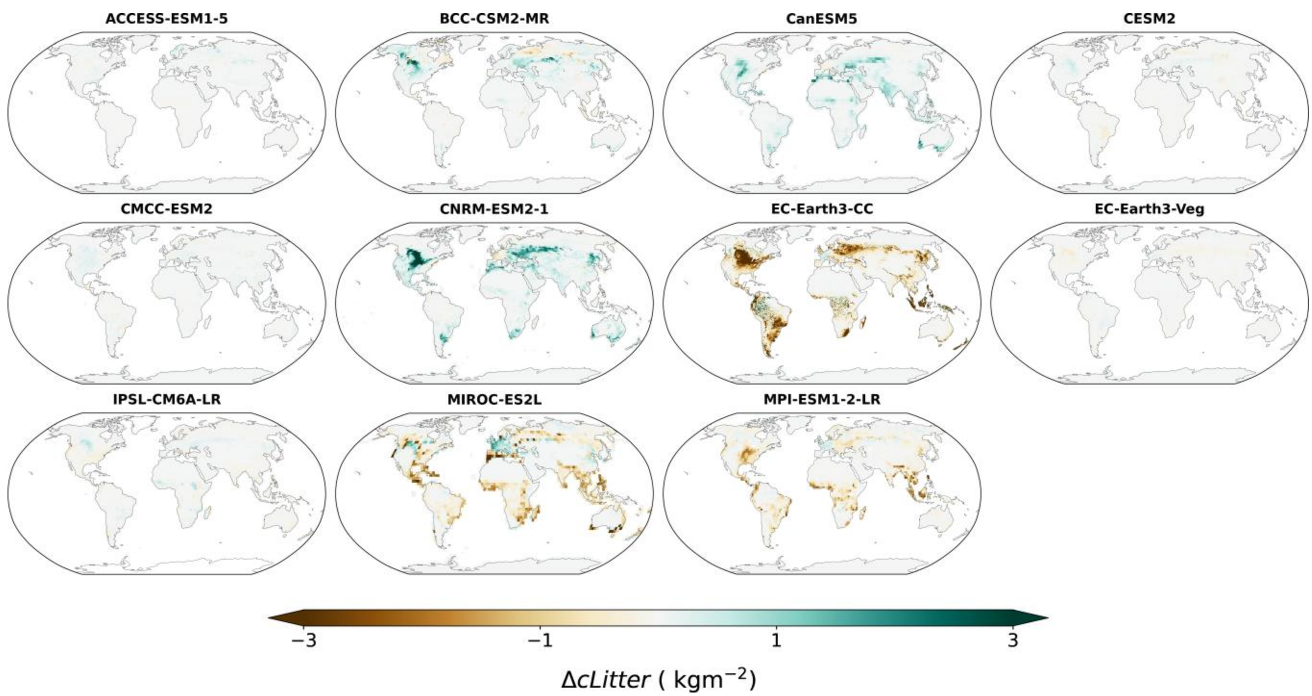

Figure S4. Change in litter carbon pools (ΔcLitter) due to land-use change. Results are computed as the running mean, centred over the last 30 years (1985–2014), from the difference between *historical* and *hist-noLu* simulations. Owing to model architecture, neither the GFDL nor the UKESM models account for carbon transitions to litter carbon pools explicitly, and those models are thus not shown.

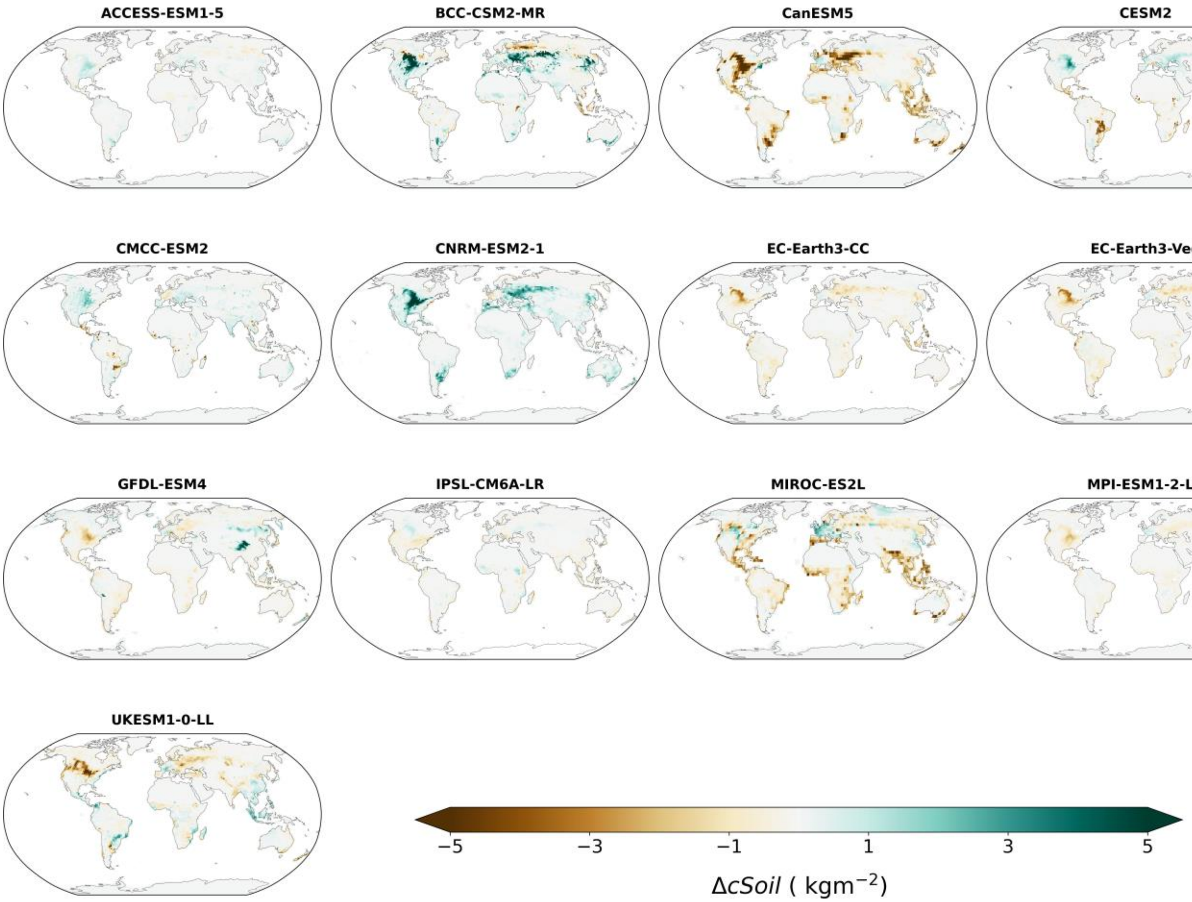

Figure S5. Change in soil carbon pools (ΔcSoil) due to land-use change. Results are computed as the running mean, centred over the last 30 years (1985–2014), from the difference between *historical* and *hist-noLu* simulations.

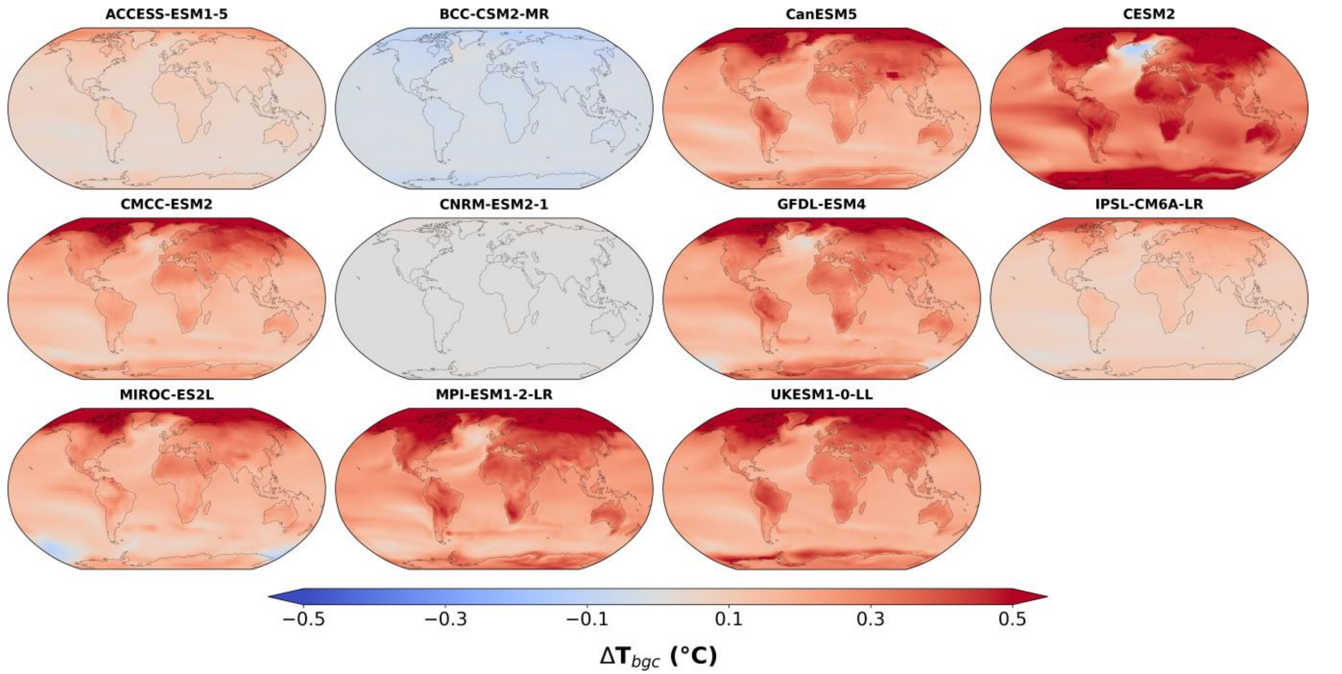

Figure S6. Temperature response (ΔT_{bgc}) to land CO_2 fluxes. Results are computed from Equations (**2**) and (**3**) using global mean land-use emissions (1985–2014), global mean temperature from the *1pctCO2* simulation, and transient climate response to cumulative emissions (TCRE) values derived in Arora et al. (2020) and Lovato et al. (2022).

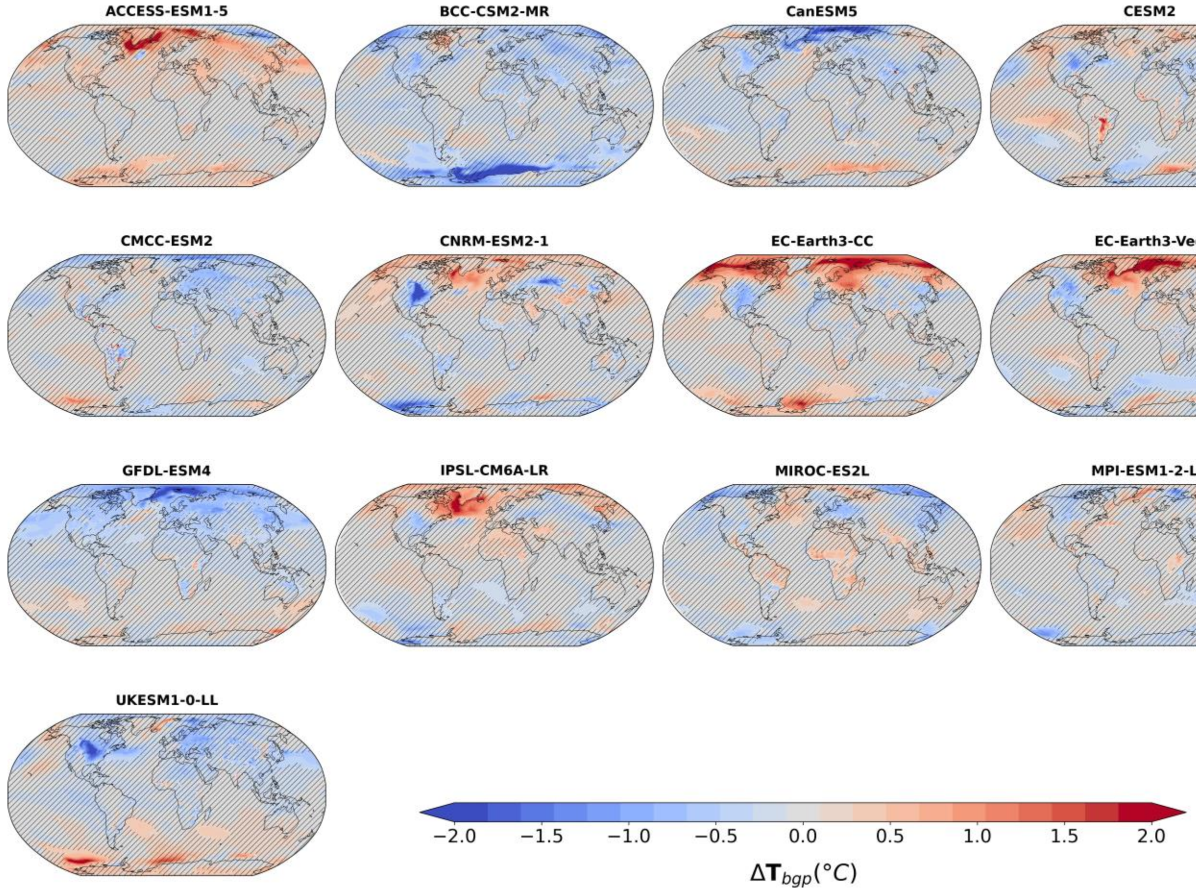

Figure S7. Response of near-surface air temperature due (ΔT_{bgc}) to biogeophysical effects of land-use change. Results computed as the mean in 1985–2014 from the difference between *historical* and *hist-noLu* experiments. Stippling indicates where results are not statistically significant at the 5% significance level using the modified Student's t-test accounting for lag-1 spatial auto-correlation (Lorenz et al., 2016; Zwiers and Von Storch, 1995).

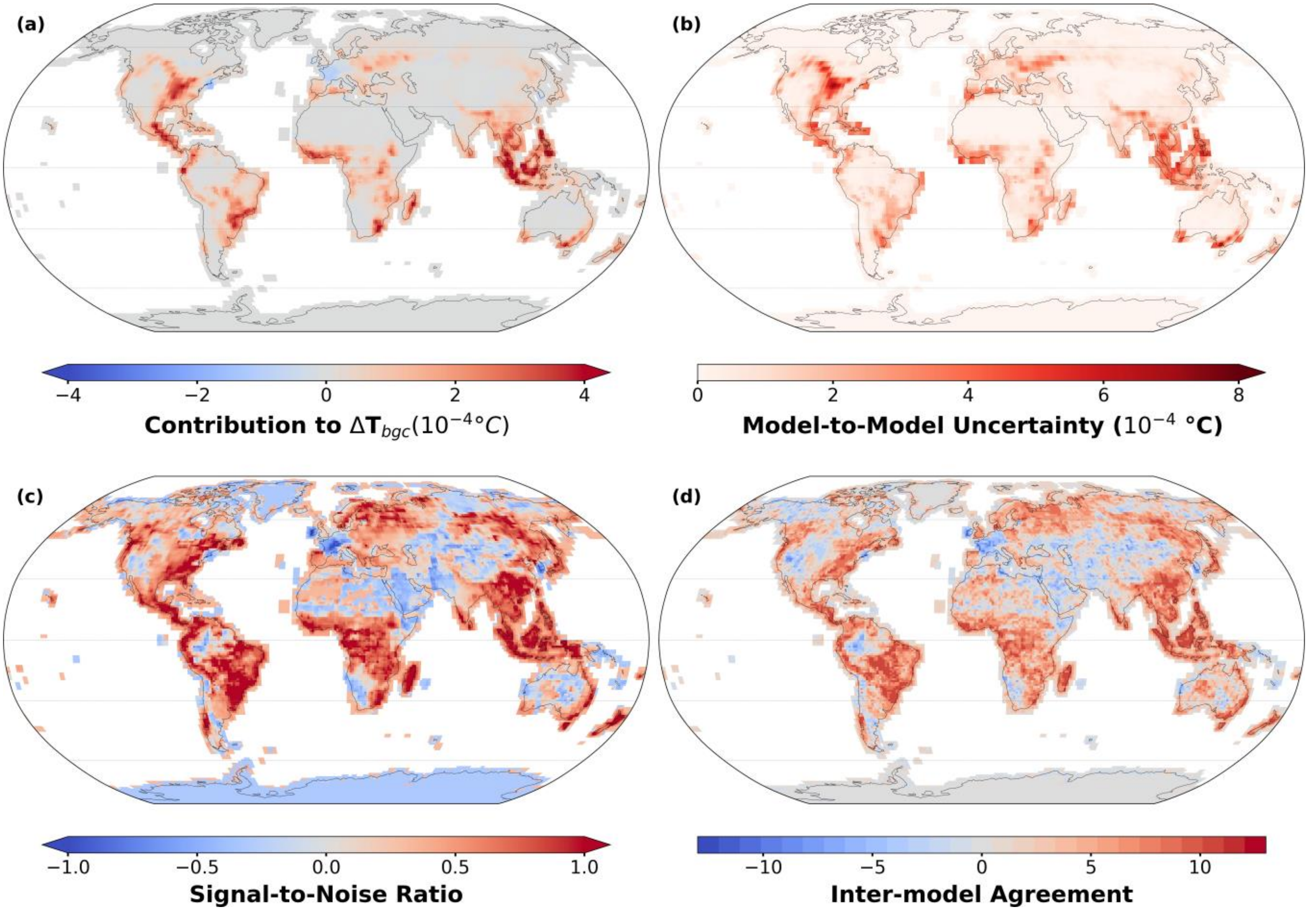

Figure S8. Local contribution of land CO_2 fluxes to global temperature change as (**a**), the multi-model mean computed as the product of the mean land-use emission per grid cell over 30 years (1985-2014) and the transient climate response to cumulative emissions value (TCRE), (**b**) the inter-model spread, computed as the standard deviation, showing the uncertainty in estimates over each grid cell. The signal-to-noise ratio (**c**) indicates the strength of the signal as compared to the inter-model uncertainty. It measures the relative weight of the multi-model mean anomalies in (**a**) with respect to the model coherence in (**b**) where a high absolute number means a robust signal. And finally, (**d**) the inter-model agreement shows the sum of the sign of ΔT_{bgc} (-1 or +1) across all models (direction, rather than magnitude) for each grid cell (blues: negative/decreasing; reds: positive/increasing). Results were computed across 11 earth system models, as the mean centred over the last 30 years (1985-2014) for each model from the difference between the *historical* and *hist-noLu* simulation.

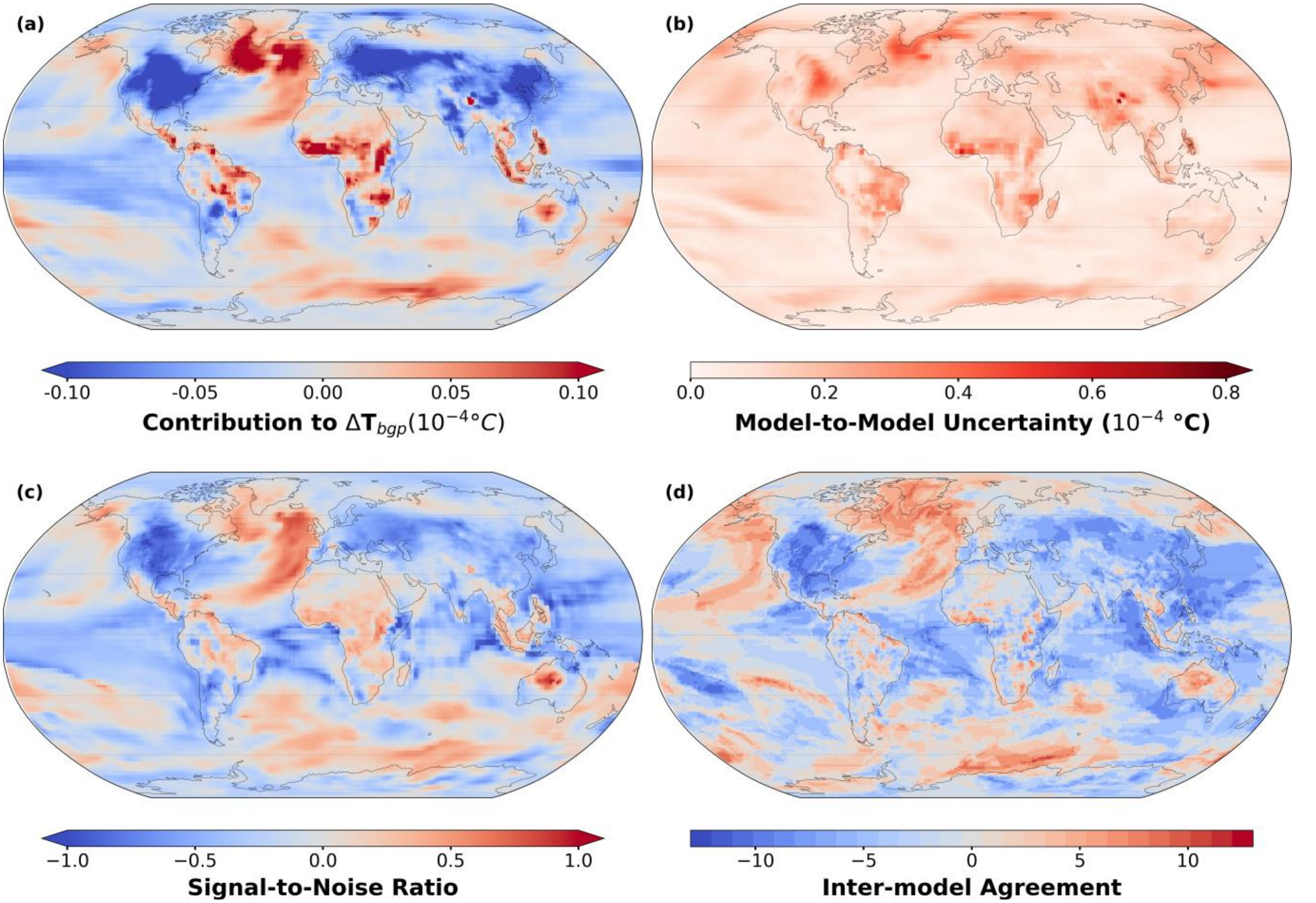

Figure S9. Local contribution of biogeophysical effects to global temperature change as (**a**), the multi-model mean computed as the product of the mean grid cell temperature over 30 years (1985-2014) and the grid cell weighted area, (**b**) the inter-model spread, computed as the standard deviation, showing the uncertainty in estimates over each grid cell. The signal-to-noise ratio (**c**) indicates the strength of the signal as compared to the inter-model uncertainty. It measures the relative weight of the multi-model mean anomalies in (**a**) with respect to the model coherence in (**b**) where a high absolute number means a robust signal. And finally, (**d**) the inter-model agreement shows the sum of the sign of ΔT_{bgp} (-1 or +1) across all models (direction, rather than magnitude) for each grid cell (blues: negative/decreasing; reds: positive/increasing). Results were computed across 13 earth system models, as the mean centred over the last 30 years (1985-2014) for each model from the difference between the *historical* and *hist-noLu* simulation.

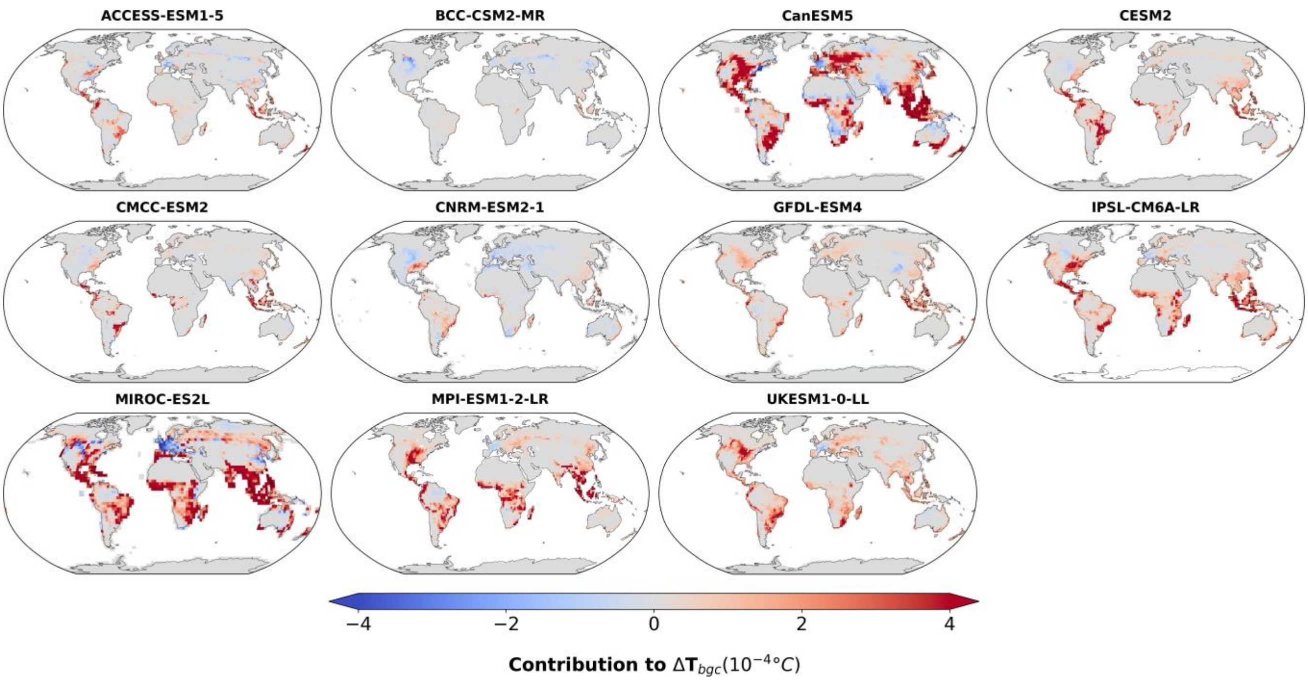

Figure S10. Local contribution of each grid cell to biogeochemical-induced global temperature change. Results are computed using grid cell mean land-use emissions (1985–2014), and transient climate response to cumulative emissions values (TCRE) derived in Arora et al. (2020)and Lovato et al. (2022) using grid cell temperature using Equation (6).

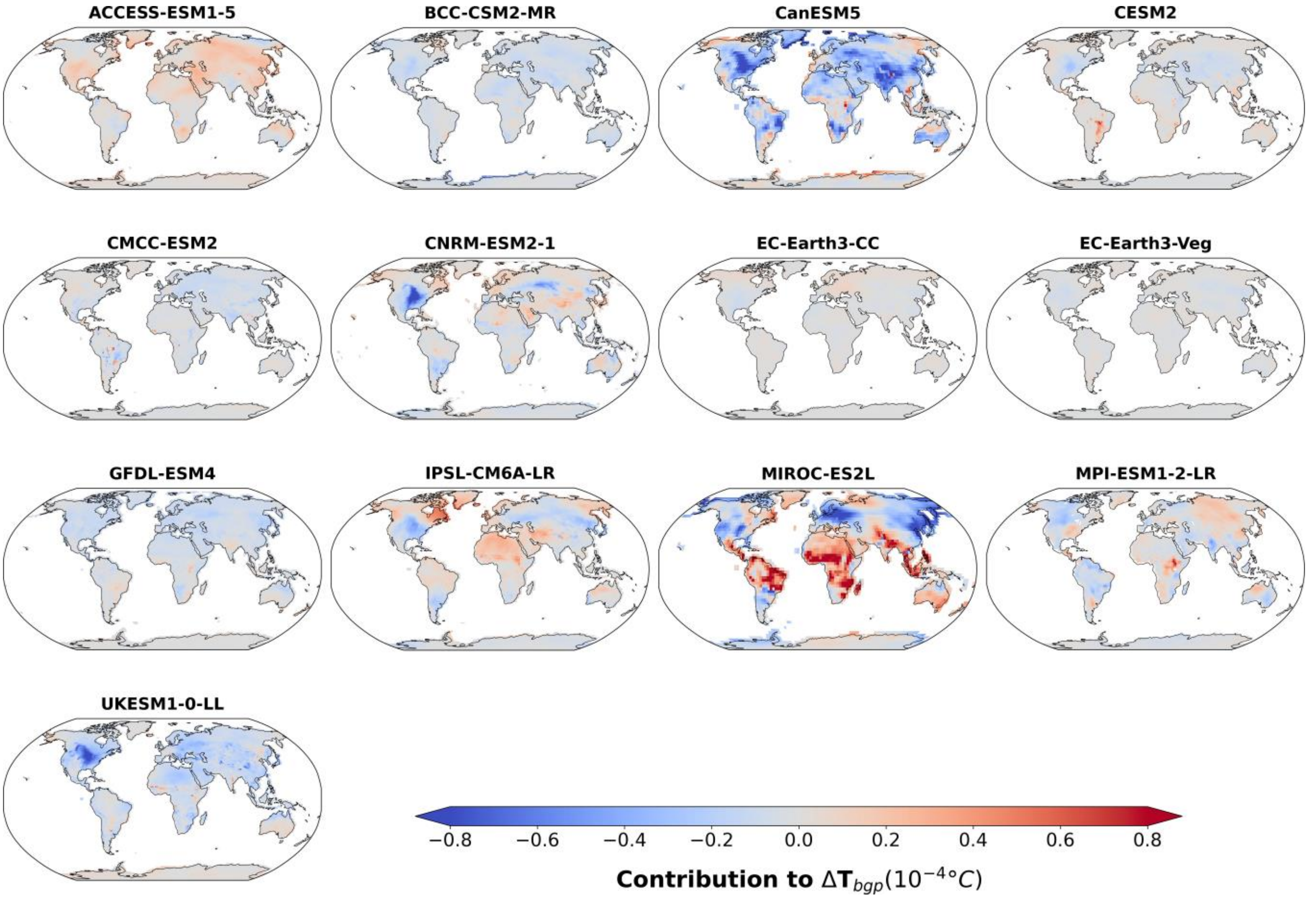

Figure S11. Local contribution of each grid cell to biogeophysical-induced global temperature change. Results are computed as the product of the weight of the grid cell area and the grid cell temperature using Equation (**7**).

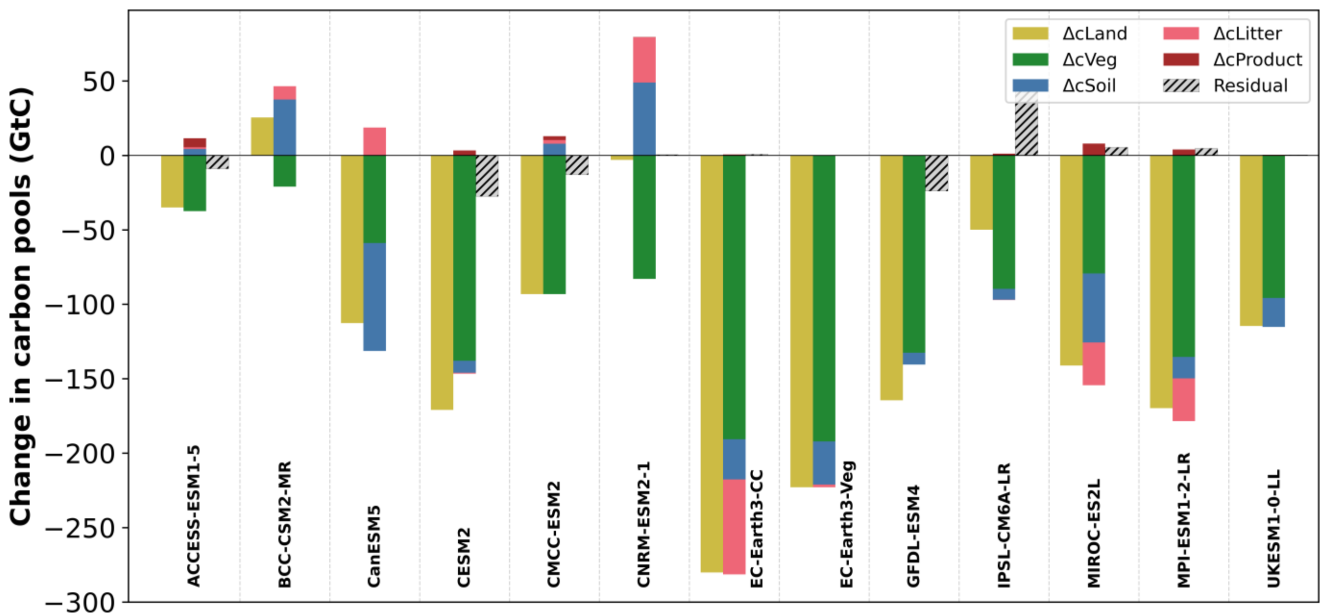

Figure S12. Variability in contributing carbon pools across Earth System Models. The average change across land carbon pools due to land- use change is computed as the mean from 1985-2014. The residual term is computed as the difference between ΔcLand and the change in the main carbon pools, cLitter, Soil, cVeg, and cProduct where available.

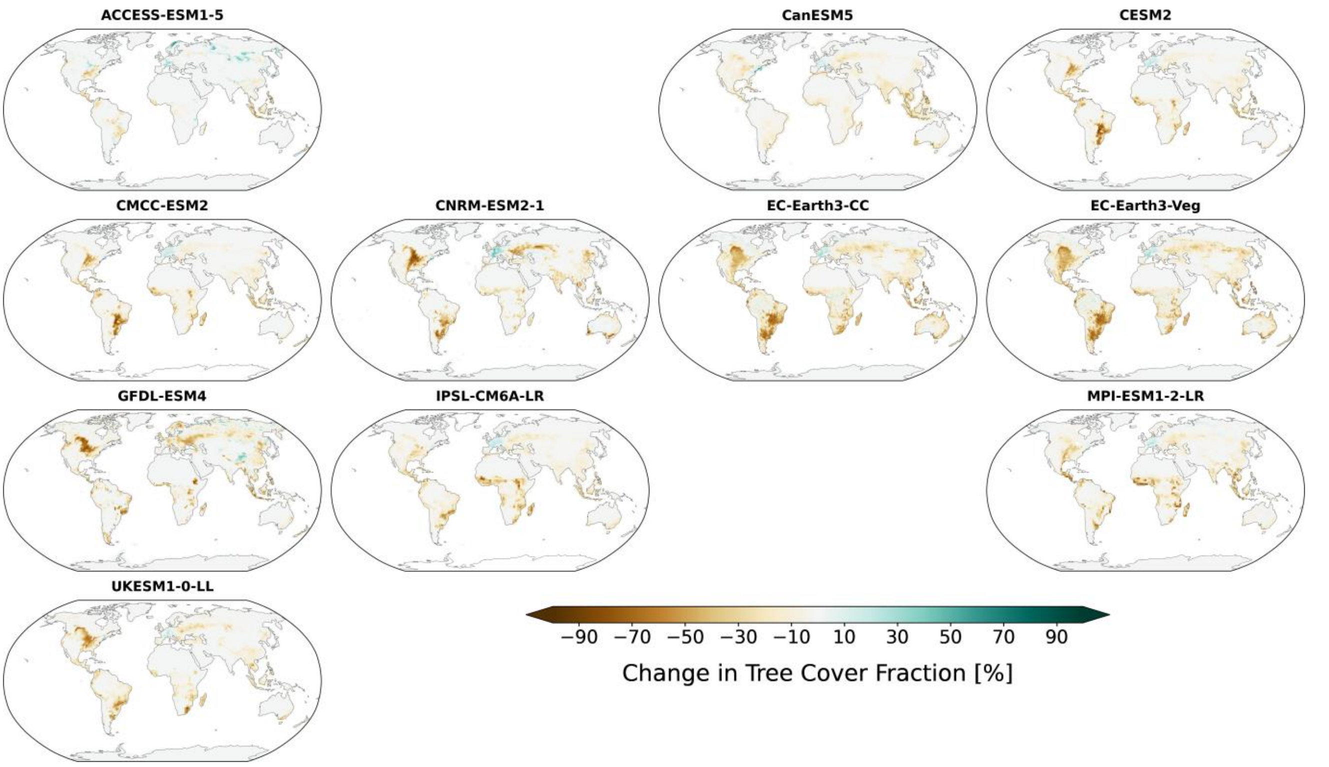

Figure S13. Change in tree cover fraction area due to land-use change in the year 2000. As the effect of natural variability is negligible, no long-term averaging is necessary.

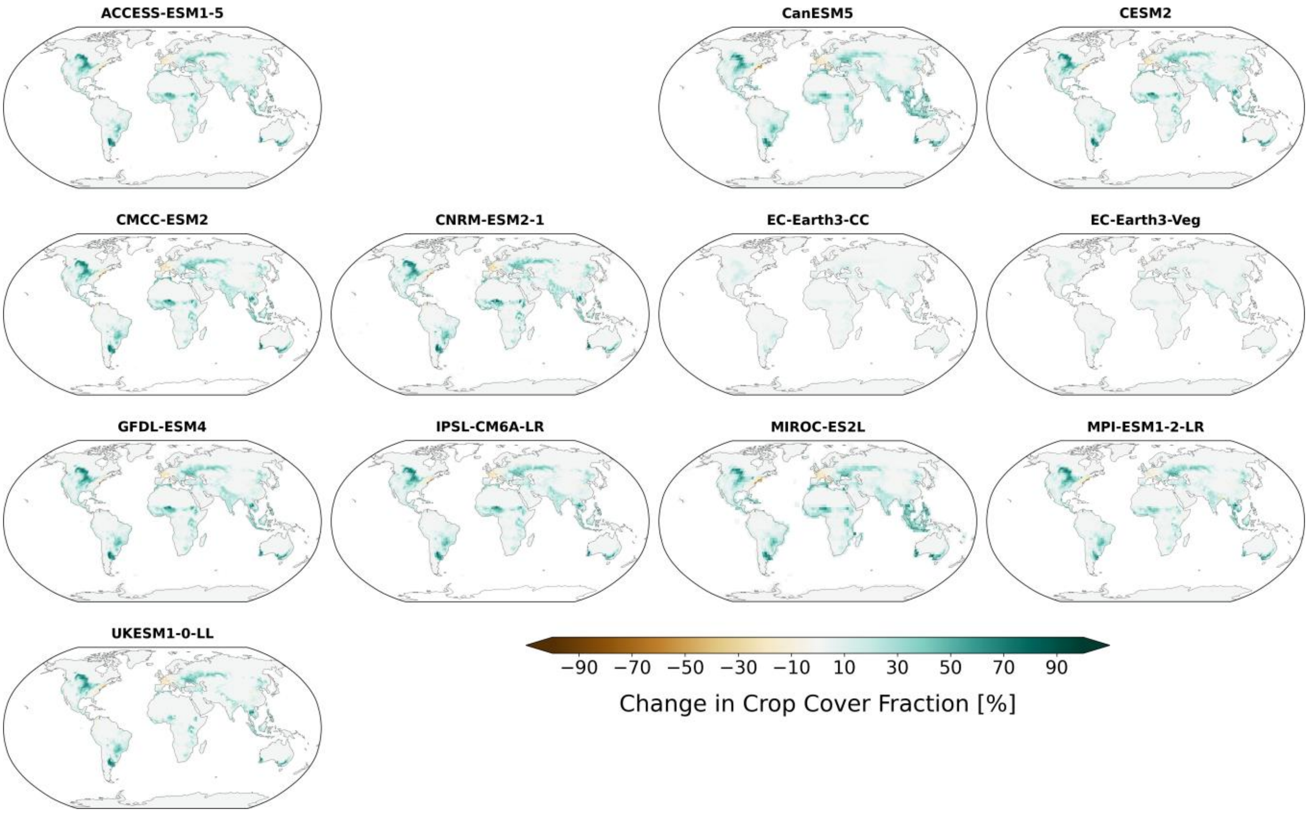

Figure S14. Change in tree cover fraction area due to land-use change in the year 2000. As the effect of natural variability is negligible, no long-term averaging is necessary.

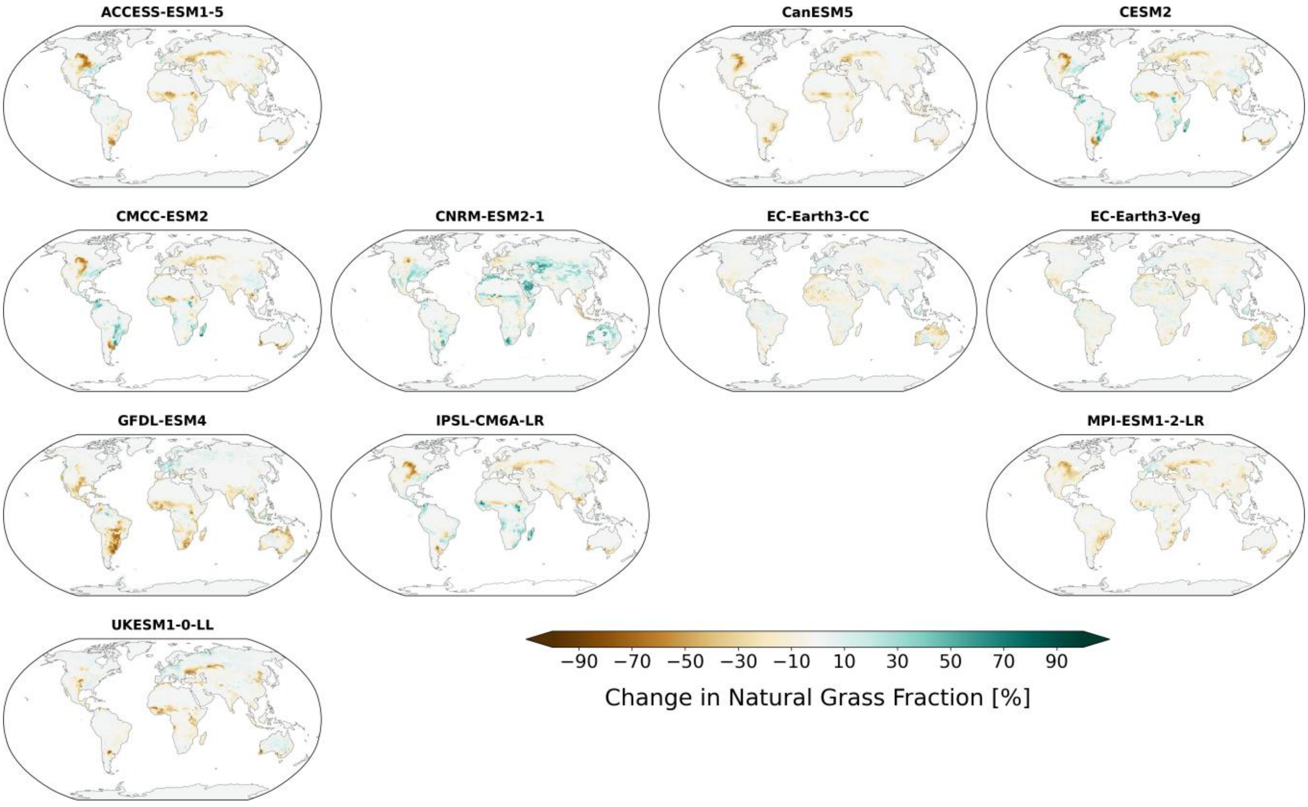

Figure S15. Change in natural grass fraction area due to land-use change in the year 2000. As the effect of natural variability is negligible, no long-term averaging is necessary.

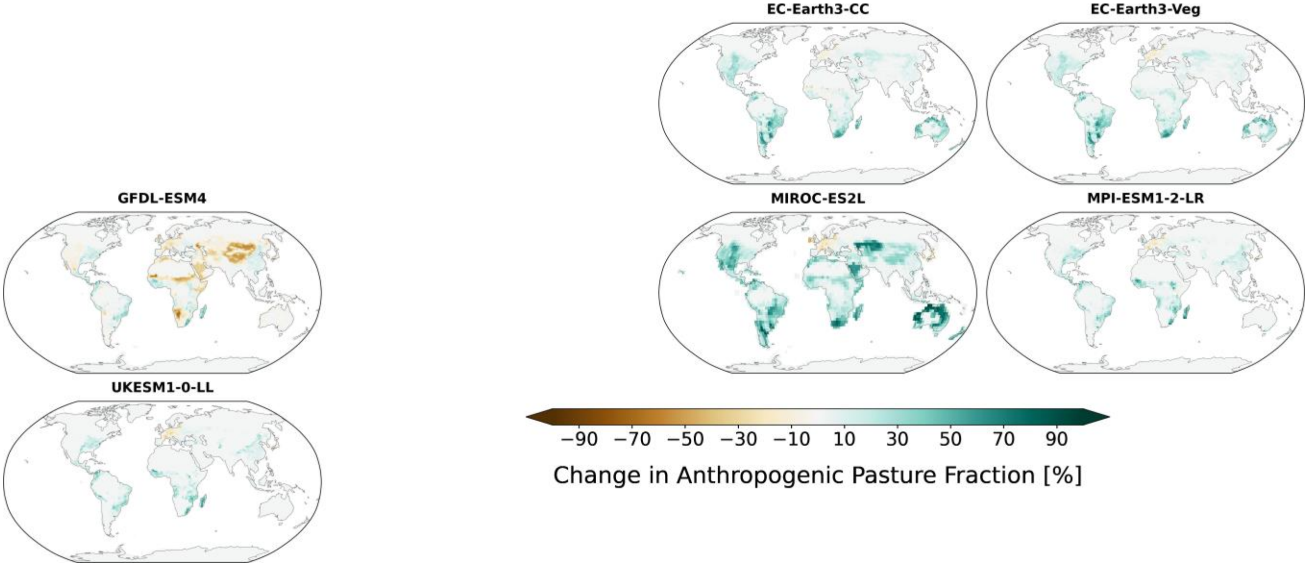

Figure S16. Change in anthropogenic pasture fraction area due to land-use change in the year 2000. As the effect of natural variability is negligible, no long-term averaging is necessary.

References

Arora, V. K., Katavouta, A., Williams, R. G., Jones, C. D., Brovkin, V., Friedlingstein, P., Schwinger, J., Bopp, L., Boucher, O., Cadule, P., Chamberlain, M. A., Christian, J. R., Delire, C., Fisher, R. A., Hajima, T., Ilyina, T., Joetzjer, E., Kawamiya, M., Koven, C. D., Krasting, J. P., Law, R. M., Lawrence, D. M., Lenton, A., Lindsay, K., Pongratz, J., Raddatz, T., Séférian, R., Tachiiri, K., Tjiputra, J. F., Wiltshire, A., Wu, T., and Ziehn, T.: Carbon–concentration and carbon–climate feedbacks in CMIP6 models and their comparison to CMIP5 models, Biogeosciences, 17, 4173–4222, https://doi.org/10.5194/bg-17-4173-2020, 2020.

Asaadi, A., Arora, V. K., Melton, J. R., and Bartlett, P.: An improved parameterization of leaf area index (LAI) seasonality in the Canadian Land Surface Scheme (CLASS) and Canadian Terrestrial Ecosystem Model (CTEM) modelling framework, Biogeosciences, 15, 6885–6907, https://doi.org/10.5194/bg-15-6885-2018, 2018.

Boysen, L. R., Brovkin, V., Pongratz, J., Lawrence, D. M., Lawrence, P., Vuichard, N., Peylin, P., Liddicoat, S., Hajima, T., Zhang, Y., Rocher, M., Delire, C., Séférian, R., Arora, V. K., Nieradzik, L., Anthoni, P., Thiery, W., Laguë, M. M., Lawrence, D., and Lo, M.-H.: Global climate response to idealized deforestation in CMIP6 models, Biogeosciences, 17, 5615–5638, https://doi.org/10.5194/bg-17-5615-2020, 2020.

Brovkin, V., Sitch, S., Von Bloh, W., Claussen, M., Bauer, E., and Cramer, W.: Role of land cover changes for atmospheric CO2 increase and climate change during the last 150 years, Global Change Biology, 10, 1253–1266, https://doi.org/10.1111/j.1365-2486.2004.00812.x, 2004.

Brovkin, V., Claussen, M., Driesschaert, E., Fichefet, T., Kicklighter, D., Loutre, M. F., Matthews, H. D., Ramankutty, N., Schaeffer, M., and Sokolov, A.: Biogeophysical effects of historical land cover changes simulated by six Earth system models of intermediate complexity, Climate Dynamics, 26, 587–600, https://doi.org/10.1007/s00382-005-0092-6, 2006.

Burton, C., Betts, R., Cardoso, M., Feldpausch, T. R., Harper, A., Jones, C. D., Kelley, D. I., Robertson, E., and Wiltshire, A.: Representation of fire, land-use change and vegetation dynamics in the Joint UK Land Environment Simulator vn4.9 (JULES), Geoscientific Model Development, 12, 179–193, https://doi.org/10.5194/gmd-12-179-2019, 2019.

Davin, E. L., de Noblet-Ducoudré, N., and Friedlingstein, P.: Impact of land cover change on surface climate: Relevance of the radiative forcing concept, Geophysical Research Letters, 34, L13 702, https://doi.org/10.1029/2007GL029678, 2007.

Delire, C., Séférian, R., Decharme, B., Alkama, R., Calvet, J., Carrer, D., Gibelin, A., Joetzjer, E., Morel, X., Rocher, M., and Tzanos, D.: The Global Land Carbon Cycle Simulated With ISBA-CTRIP: Improvements Over the Last Decade, Journal of Advances in Modeling Earth Systems, 12, e2019MS001 886, https://doi.org/10.1029/2019MS001886, 2020.

Devaraju, N., Tharammal, T., and Bala, G.: Biophysical and biogeochemical effects of historical and future scenarios of anthropogenic land cover change on climate, https://doi.org/10.21203/rs.3.rs-2292826/v1, 2022.

Eby, M., Weaver, A. J., Alexander, K., Zickfeld, K., Abe-Ouchi, A., Cimatoribus, A. A., Crespin, E., Drijfhout, S. S., Edwards, N. R., Eliseev, A. V., Feulner, G., Fichefet, T., Forest, C. E., Goosse, H., Holden, P. B., Joos, F., Kawamiya, M., Kicklighter, D., Kienert, H., Matsumoto, K., Mokhov, I. I., Monier, E., Olsen, S. M., Pedersen, J. O. P., Perrette, M., Philippon-Berthier, G., Ridgwell, A., Schlosser, A., Schneider von Deimling, T., Shaffer, G., Smith, R. S., Spahni, R., Sokolov, A. P., Steinacher, M., Tachiiri, K., Tokos, K., Yoshimori, M., Zeng, N., and Zhao, F.: Historical and idealized climate model experiments: an intercomparison of Earth system models of intermediate complexity, Climate of the Past, 9, 1111–1140, https://doi.org/10.5194/cp-9-1111-2013, 2013.

Friedlingstein, P., O'Sullivan, M., Jones, M. W., Andrew, R. M., Bakker, D. C. E., Hauck, J., Landschützer, P., Le Quéré, C., Luijkx, I. T., Peters, G. P., Peters, W., Pongratz, J., Schwingshackl, C., Sitch, S., Canadell, J. G., Ciais, P., Jackson, R. B., Alin, S. R., Anthoni, P., Barbero, L., Bates, N. R., Becker, M., Bellouin, N., Decharme, B., Bopp, L., Brasika, I. B. M., Cadule, P., Chamberlain, M. A., Chandra, N., Chau, T.-T.-T., Chevallier, F., Chini, L. P., Cronin, M., Dou, X., Enyo, K., Evans, W., Falk, S., Feely, R. A., Feng, L., Ford, D. J., Gasser, T., Ghattas, J., Gkritzalis, T., Grassi, G., Gregor, L., Gruber, N., Gürses, Harris, I., Hefner, M., Heinke, J., Houghton, R. A., Hurtt, G. C., Iida, Y., Ilyina, T., Jacobson, A. R., Jain, A., Jarníková, T., Jersild, A., Jiang, F., Jin, Z., Joos, F., Kato, E., Keeling, R. F., Kennedy, D., Klein Goldewijk, K., Knauer, J., Korsbakken, J. I., Körtzinger, A., Lan, X., Lefèvre, N., Li, H., Liu, J., Liu, Z., Ma, L., Marland, G., Mayot, N., McGuire, P. C., McKinley, G. A., Meyer, G., Morgan, E. J., Munro, D. R., Nakaoka, S.-I., Niwa, Y., O'Brien, K. M., Olsen, A., Omar, A. M., Ono, T., Paulsen, M., Pierrot, D., Pocock, K., Poulter, B., Powis, C. M., Rehder, G., Resplandy, L., Robertson, E., Rödenbeck, C., Rosan, T. M., Schwinger, J., Séférian, R., Smallman, T. L., Smith, S. M., Sospedra-Alfonso, R., Sun, Q., Sutton, A. J., Sweeney, C., Takao, S., Tans, P. P., Tian, H., Tilbrook, B., Tsujino, H., Tubiello, F., van der Werf, G. R., van Ooijen, E., Wanninkhof, R., Watanabe, M., Wimart-Rousseau, C., Yang, D., Yang, X., Yuan, W., Yue, X., Zaehle, S., Zeng, J., and Zheng, B.: Global Carbon Budget 2023, Earth System Science Data, 15, 5301–5369, https://doi.org/10.5194/essd-15-5301-2023, 2023.

Haverd, V., Smith, B., Nieradzik, L., Briggs, P. R., Woodgate, W., Trudinger, C. M., Canadell, J. G., and Cuntz, M.: A new version of the CABLE land surface model (Subversion revision r4601) incorporating land use and land cover change, woody vegetation demography, and a novel optimisation-based approach to plant coordination of photosynthesis, Geoscientific Model Development, 11, 2995–3026, https://doi.org/10.5194/gmd-11-2995-2018, 2018

Heinke, J., Rolinski, S., and Müller, C.: Modelling the role of livestock grazing in C and N cycling in grasslands with LPJmL5.0-grazing, Geoscientific Model Development, 16, 2455–2475, https://doi.org/10.5194/gmd-16-2455-2023, 2023.

Ito, A. and Inatomi, M.: Use of a process-based model for assessing the methane budgets of global terrestrial ecosystems and evaluation of uncertainty, Biogeosciences, 9, 759–773, https://doi.org/10.5194/bg-9-759-2012, 2012.

Jain, A. K., Meiyappan, P., Song, Y., and House, J. I.: emissions from land-use change affected more by nitrogen cycle, than by the choice of land-cover data, Global Change Biology, 19, 2893–2906, https://doi.org/10.1111/gcb.12207, 2013.

Jia, G., Shevliakova, E., Artaxo, P., Noblet-Ducoudré, N. D., Houghton, R., House, J., Kitajima, K., Lennard, C., Popp, A., Sirin, A., Sukumar, R., and Verchot, L.: Land–climate interactions, in: Climate Change and Land: an IPCC Special Report on Climate Change, Desertification, Land Degradation, Sustainable Land Management, Food Security, and Greenhouse Gas Fluxes in Terrestrial Ecosystems, edited by Shukla, P. R., Skea, J., Buendía, E. C., Masson-Delmotte, V., Pörtner, H.-O., Roberts, D. C., Zhai, P., Slade, R., Connors, S. L., Diemen, R. v., Ferrat, M., Haughey, E., Luz, S., Neogi, S., Pathak, M., Petzold, J., Portugal Pereira, J., Vyas, P., Huntley, E., Kissick, K., Belkacemi, M., and Malley, J., pp. 131–248, Cambridge University Press, 1 edn., https://doi.org/10.1017/9781009157988.004, 2019.

Kato, E., Kinoshita, T., Ito, A., Kawamiya, M., and Yamagata, Y.: Evaluation of spatially explicit emission scenario of land-use change and biomass burning using a process-based biogeochemical model, Journal of Land Use Science, 8, 104–122, https://doi.org/10.1080/1747423X.2011.628705, 2013.

Krinner, G., Viovy, N., de Noblet-Ducoudré, N., Ogée, J., Polcher, J., Friedlingstein, P., Ciais, P., Sitch, S., and Prentice, I. C.: A dynamic global vegetation model for studies of the coupled atmosphere-biosphere system, Global Biogeochemical Cycles, 19, GB1015, https://doi.org/10.1029/2003GB002199, 2005.

Lawrence, D. M., Fisher, R. A., Koven, C. D., Oleson, K. W., Swenson, S. C., Bonan, G., Collier, N., Ghimire, B., Van Kampenhout, L., Kennedy, D., Kluzek, E., Lawrence, P. J., Li, F., Li, H., Lombardozzi, D., Riley, W. J., Sacks, W. J., Shi, M., Vertenstein, M., Wieder, W. R., Xu, C., Ali, A. A., Badger, A. M., Bisht, G., Van Den Broeke, M., Brunke, M. A., Burns, S. P., Buzan, J., Clark, M., Craig, A., Dahlin, K., Drewniak, B., Fisher, J. B., Flanner, M., Fox, A. M., Gentine, P., Hoffman, F., Keppel-Aleks, G., Knox, R., Kumar, S., Lenaerts, J., Leung, L. R., Lipscomb, W. H., Lu, Y., Pandey, A., Pelletier, J. D., Perket, J., Randerson, J. T., Ricciuto, D. M., Sanderson, B. M., Slater, A., Subin, Z. M., Tang, J., Thomas, R. Q., Val Martin, M., and Zeng, X.: The Community Land Model Version 5: Description of New Features, Benchmarking, and Impact of Forcing Uncertainty, Journal of Advances in Modeling Earth Systems, 11, 4245–4287, https://doi.org/10.1029/2018MS001583, 2019.

Lawrence, P. J., Feddema, J. J., Bonan, G. B., Meehl, G. A., O'Neill, B. C., Oleson, K. W., Levis, S., Lawrence, D. M., Kluzek, E., Lindsay, K., and Thornton, P. E.: Simulating the Biogeochemical and Biogeophysical Impacts of Transient Land Cover Change and Wood Harvest in the Community Climate System Model (CCSM4) from 1850 to 2100, Journal of Climate, 25, 3071–3095, https://doi.org/10.1175/JCLI-D-11-00256.1, 2012.

Lienert, S. and Joos, F.: A Bayesian ensemble data assimilation to constrain model parameters and land-use carbon emissions, Biogeosciences, 15, 2909–2930, https://doi.org/10.5194/bg-15-2909-2018, 2018.

Lombardozzi, D. L., Lu, Y., Lawrence, P. J., Lawrence, D. M., Swenson, S., Oleson, K. W., Wieder, W. R., and Ainsworth, E. A.: Simulating Agriculture in the Community Land Model Version 5, Journal of Geophysical Research: Biogeosciences, 125, e2019JG005 529, https://doi.org/10.1029/2019JG005529, 2020.

Lorenz, R., Pitman, A. J., and Sisson, S. A.: Does Amazonian deforestation cause global effects; can we be sure?, Journal of Geophysical Research: Atmospheres, 121, 5567–5584, https://doi.org/10.1002/2015JD024357, 2016.

Lovato, T., Peano, D., Butenschön, M., Materia, S., Iovino, D., Scoccimarro, E., Fogli, P. G., Cherchi, A., Bellucci, A., Gualdi, S., Masina, S., and Navarra, A.: CMIP6 Simulations With the CMCC Earth System Model (CMCC-ESM2), Journal of Advances in Modeling Earth Systems, 14, e2021MS002 814, https://doi.org/10.1029/2021MS002814, 2022.

Lutz, F., Herzfeld, T., Heinke, J., Rolinski, S., Schaphoff, S., von Bloh, W., Stoorvogel, J. J., and Müller, C.:

Simulating the effect of tillage practices with the global ecosystem model LPJmL (version 5.0-tillage), Geoscientific Model Development, 12, 2419–2440, https://doi.org/10.5194/gmd-12-2419-2019, 2019.

Matthews, H. D., Weaver, A. J., Meissner, K. J., Gillett, N. P., and Eby, M.: Natural and anthropogenic climate change: incorporating historical land cover change, vegetation dynamics and the global carbon cycle, Climate Dynamics, 22, 461–479, https://doi.org/10.1007/s00382-004-0392-2, 2004.

Mauritsen, T., Bader, J., Becker, T., Behrens, J., Bittner, M., Brokopf, R., Brovkin, V., Claussen, M., Crueger, T., Esch, M., Fast, I., Fiedler, S., Fläschner, D., Gayler, V., Giorgetta, M., Goll, D. S., Haak, H., Hagemann, S., Hedemann, C., Hohenegger, C., Ilyina, T., Jahns, T., Jimenéz-de-la-Cuesta, D., Jungclaus, J., Kleinen, T., Kloster, S., Kracher, D., Kinne, S., Kleberg, D., Lasslop, G., Kornblueh, L., Marotzke, J., Matei, D., Meraner, K., Mikolajewicz, U., Modali, K., Möbis, B., Müller, W. A., Nabel, J. E. M. S., Nam, C. C. W., Notz, D., Nyawira, S., Paulsen, H., Peters, K., Pincus, R., Pohlmann, H., Pongratz, J., Popp, M., Raddatz, T. J., Rast, S., Redler, R., Reick, C. H., Rohrschneider, T., Schemann, V., Schmidt, H., Schnur, R., Schulzweida, U., Six, K. D., Stein, L., Stemmler, I., Stevens, B., Storch, J., Tian, F., Voigt, A., Vrese, P., Wieners, K., Wilkenskjeld, S., Winkler, A., and Roeckner, E.: Developments in the MPI-M Earth System Model version 1.2 (MPI-ESM1.2) and Its Response to Increasing CO 2, Journal of Advances in Modeling Earth Systems, 11, 998–1038, https://doi.org/10.1029/2018MS001400, 2019.

Meiyappan, P., Jain, A. K., and House, J. I.: Increased influence of nitrogen limitation on CO2 emissions from future land use and land use change, Global Biogeochemical Cycles, 29, 1524–1548, https://doi.org/10.1002/2015GB005086, 2015.

Melton, J. R., Arora, V. K., Wisernig-Cojoc, E., Seiler, C., Fortier, M., Chan, E., and Teckentrup, L.: CLASSIC v1.0: the open-source community successor to the Canadian Land Surface Scheme (CLASS) and the Canadian Terrestrial Ecosystem Model (CTEM) – Part 1: Model framework and site-level performance, Geoscientific Model Development, 13, 2825–2850, https://doi.org/10.5194/gmd-13-2825-2020, 2020.

Pongratz, J., Reick, C. H., Raddatz, T., and Claussen, M.: Effects of anthropogenic land cover change on the carbon cycle of the last millennium, Global Biogeochemical Cycles, 23, GB4001, https://doi.org/10.1029/2009GB003488, 2009.

Pongratz, J., Reick, C. H., Raddatz, T., and Claussen, M.: Biogeophysical versus biogeochemical climate response to historical anthropogenic land cover change: CLIMATE EFFECTS OF HISTORICAL LAND COVER CHANGE, Geophysical Research Letters, 37, L08 702, https://doi.org/10.1029/2010GL043010, 2010.

Poulter, B., Frank, D. C., Hodson, E. L., and Zimmermann, N. E.: Impacts of land cover and climate data selection on understanding terrestrial carbon dynamics and the CO2 airborne fraction, Biogeosciences, 8, 2027–2036, https://doi.org/10.5194/bg-8-2027-2011, 2011.

Reick, C. H., Gayler, V., Goll, D., Hagemann, S., Heidkamp, M., Nabel, J. E. M. S., Raddatz, T., Roeckner, E., Schnur, R., and Wilkenskjeld, S.: JSBACH 3 - The land component of the MPI Earth System Model: documentation of version 3.2, Reports on Earth System Science, p. 272, https://doi.org/10.17617/2.3279802, 2021.

Schaphoff, S., von Bloh, W., Rammig, A., Thonicke, K., Biemans, H., Forkel, M., Gerten, D., Heinke, J., Jägermeyr, J., Knauer, J., Langerwisch, F., Lucht, W., Müller, C., Rolinski, S., and Waha, K.: LPJmL4

– a dynamic global vegetation model with managed land – Part 1: Model description, Geoscientific Model Development, 11, 1343–1375, https://doi.org/10.5194/gmd-11-1343-2018, 2018.

Sellar, A. A., Jones, C. G., Mulcahy, J. P., Tang, Y., Yool, A., Wiltshire, A., O'Connor, F. M., Stringer, M., Hill, R., Palmieri, J., Woodward, S., Mora, L., Kuhlbrodt, T., Rumbold, S. T., Kelley, D. I., Ellis, R., Johnson, C. E., Walton, J., Abraham, N. L., Andrews, M. B., Andrews, T., Archibald, A. T., Berthou, S., Burke, E., Blockley, E., Carslaw, K., Dalvi, M., Edwards, J., Folberth, G. A., Gedney, N., Griffiths, P. T., Harper, A. B., Hendry, M. A., Hewitt, A. J., Johnson, B., Jones, A., Jones, C. D., Keeble, J., Liddicoat, S., Morgenstern, O., Parker, R. J., Predoi, V., Robertson, E., Siahaan, A., Smith, R. S., Swaminathan, R., Woodhouse, M. T., Zeng, G., and Zerroukat, M.: UKESM1: Description and Evaluation of the U.K. Earth System Model, Journal of Advances in Modeling Earth Systems, 11, 4513–4558, https://doi.org/10.1029/2019MS001739, 2019.

Shi, Z., Yan, X., Yin, C., and Wang, Z.: Effects of historical land cover changes on climate, Chinese Science Bulletin, 52, 2575–2583, https://doi.org/10.1007/s11434-007-0381-z, 2007.

Shi, Z., Hoffman, F. M., Xu, M., Mishra, U., Allison, S. D., Zhou, J., and Randerson, J. T.: Global-Scale Convergence Obscures Inconsistencies in Soil Carbon Change Predicted by Earth System Models, AGU Advances, 5, e2023AV001 068, https://doi.org/10.1029/2023AV001068, 2024.

Shu, S., Jain, A. K., Koven, C. D., and Mishra, U.: Estimation of Permafrost SOC Stock and Turnover Time Using a Land Surface Model With Vertical Heterogeneity of Permafrost Soils, Global Biogeochemical Cycles, 34, e2020GB006 585, https://doi.org/10.1029/2020GB006585, 2020.

Simmons, C. T. and Matthews, H. D.: Assessing the implications of human land-use change for the transient climate response to cumulative carbon emissions, Environmental Research Letters, 11, 035 001, https://doi.org/10.1088/1748-9326/11/3/035001, 2016.

Sitch, S., Friedlingstein, P., Gruber, N., Jones, S. D., Murray-Tortarolo, G., Ahlström, A., Doney, S. C., Graven, H., Heinze, C., Huntingford, C., Levis, S., Levy, P. E., Lomas, M., Poulter, B., Viovy, N., Zaehle, S., Zeng, N., Arneth, A., Bonan, G., Bopp, L., Canadell, J. G., Chevallier, F., Ciais, P., Ellis, R., Gloor, M., Peylin, P., Piao, S. L., Le Quéré, C., Smith, B., Zhu, Z., and Myneni, R.: Recent trends and drivers of regional sources and sinks of carbon dioxide, Biogeosciences, 12, 653–679, https://doi.org/10.5194/bg-12-653-2015, 2015.

Smith, B., Wårlind, D., Arneth, A., Hickler, T., Leadley, P., Siltberg, J., and Zaehle, S.: Implications of incorporating N cycling and N limitations on primary production in an individual-based dynamic vegetation model, Biogeosciences, 11, 2027–2054, https://doi.org/10.5194/bg-11-2027-2014, 2014.

Tian, H., Xu, X., Lu, C., Liu, M., Ren, W., Chen, G., Melillo, J., and Liu, J.: Net exchanges of CO2, CH4, and N2O between China's terrestrial ecosystems and the atmosphere and their contributions to global climate warming, Journal of Geophysical Research: Biogeosciences, 116, G02 011, https://doi.org/10.1029/2010JG001393, 2011.

Tian, H., Lu, C., Yang, J., Banger, K., Huntzinger, D. N., Schwalm, C. R., Michalak, A. M., Cook, R., Ciais, P., Hayes, D., Huang, M., Ito, A., Jain, A. K., Lei, H., Mao, J., Pan, S., Post, W. M., Peng, S., Poulter, B., Ren, W., Ricciuto, D., Schaefer, K., Shi, X., Tao, B., Wang, W., Wei, Y., Yang, Q., Zhang, B., and Zeng, N.: Global patterns and controls of soil organic carbon dynamics as simulated by multiple terrestrial biosphere models: Current status and future directions, Global Biogeochemical Cycles, 29, 775–792, https://doi.org/10.1002/2014GB005021, 2015.

von Bloh, W., Schaphoff, S., Müller, C., Rolinski, S., Waha, K., and Zaehle, S.: Implementing the nitrogen cycle into the dynamic global vegetation, hydrology, and crop growth model LPJmL (version 5.0), Geoscientific Model Development, 11, 2789–2812, https://doi.org/10.5194/gmd-11-2789-2018, 2018.

Vuichard, N., Messina, P., Luyssaert, S., Guenet, B., Zaehle, S., Ghattas, J., Bastrikov, V., and Peylin, P.: Accounting for carbon and nitrogen interactions in the global terrestrial ecosystem model ORCHIDEE (trunk version, rev 4999): multi-scale evaluation of gross primary production, Geoscientific Model Development, 12, 4751–4779, https://doi.org/10.5194/gmd-12-4751-2019, 2019.

Walker, A. P., Quaife, T., van Bodegom, P. M., De Kauwe, M. G., Keenan, T. F., Joiner, J., Lomas, M. R., MacBean, N., Xu, C., Yang, X., and Woodward, F. I.: The impact of alternative trait-scaling hypotheses for the maximum photosynthetic carboxylation rate (Vcmax) on global gross primary production, New Phytologist, 215, 1370–1386, https://doi.org/10.1111/nph.14623, 2017.

Wang, Y., Yan, X., and Wang, Z.: The biogeophysical effects of extreme afforestation in modeling future climate, Theoretical and Applied Climatology, 118, 511–521, https://doi.org/10.1007/s00704-013-1085-8, 2014.

Wei, X., Shao, M., Gale, W., and Li, L.: Global pattern of soil carbon losses due to the conversion of forests to agricultural land, Scientific Reports, 4, 4062, https://doi.org/10.1038/srep04062, 2014.

Wiltshire, A. J., Burke, E. J., Chadburn, S. E., Jones, C. D., Cox, P. M., Davies-Barnard, T., Friedlingstein, P., Harper, A. B., Liddicoat, S., Sitch, S., and Zaehle, S.: JULES-CN: a coupled terrestrial carbon–nitrogen scheme (JULES vn5.1), Geoscientific Model Development, 14, 2161–2186, https://doi.org/10.5194/gmd-14-2161-2021, 2021.

Woodward, F. I. and Lomas, M. R.: Vegetation dynamics – simulating responses to climatic change, Biological Reviews, 79, 643–670, https://doi.org/10.1017/S1464793103006419, 2004.

Yuan, W., Liu, D., Dong, W., Liu, S., Zhou, G., Yu, G., Zhao, T., Feng, J., Ma, Z., Chen, J., Chen, Y., Chen, S., Han, S., Huang, J., Li, L., Liu, H., Liu, S., Ma, M., Wang, Y., Xia, J., Xu, W., Zhang, Q., Zhao, X., and Zhao, L.: Multiyear precipitation reduction strongly decreases carbon uptake over northern China, Journal of Geophysical Research: Biogeosciences, 119, 881–896, https://doi.org/10.1002/2014JG002608, 2014.

Yue, X. and Unger, N.: The Yale Interactive terrestrial Biosphere model version 1.0: description, evaluation and implementation into NASA GISS ModelE2, Geoscientific Model Development, 8, 2399–2417, https://doi.org/10.5194/gmd-8-2399-2015, 2015.

Zaehle, S. and Friend, A. D.: Carbon and nitrogen cycle dynamics in the O-CN land surface model: 1. Model description, site-scale evaluation, and sensitivity to parameter estimates, Global Biogeochemical Cycles, 24, GB1005, https://doi.org/10.1029/2009GB003521, 2010.

Zwiers, F. W. and Von Storch, H.: Taking Serial Correlation into Account in Tests of the Mean, Journal of Climate, 8, 336–351, https://doi.org/10.1175/1520-0442(1995)008<0336:TSCIAI>2.0.CO;2, 1995